Research Article | Vol. 26, No. 3 | 5 Feb 2018 | OPTICS EXPRESS 3604
Optics EXPRESS

Spectrometer-based refractive index and dispersion measurement using low-coherence interferometry with confocal scanning

DANIEL FRANCIS, HELEN D. FORD, AND RALPH P. TATAM*

Engineering Photonics, Cranfield University, Bedfordshire, MK43 0AL, UK
r.p.tatam@cranfield.ac.uk

Abstract: This paper describes a technique for measuring refractive index and thickness of transparent plates using a fibre-optic low-coherence interferometer. The interferometer is used to independently measure quantities related to the phase and group refractive indices, n_p and n_g, of the material under investigation. Additionally, the dispersion of the phase index dependent quantity is measured by taking advantage of the range of wavelengths available from a broadband source. These three quantities are related to simultaneously yield n_p and n_g as well as the geometrical thickness t of the sample. Measurements are presented for a range of transparent materials including measurements of the ordinary and extraordinary refractive indices of a birefringent sapphire window. The mean percentage errors across all the samples tested were 0.09% for n_p, 0.08% for n_p, and 0.11% for t.

OCIS codes: (120.0120) Instrumentation, measurement, and metrology; (120.3180) Interferometry; (180.1790) Confocal microscopy; (260.2030) Dispersion.

References and links

1. B. L. Danielson, and C. D. Whittenberg, "Guided wave reflectometry with micrometer resolution," Appl. Opt. **26**(14), 2836–2842 (1987).
2. D. Huang, E. A. Swanson, C. P. Lin, J. S. Schuman, W. G. Stinson, W. Chang, M. R. Hee, T. Flotte, K. Gregory, C. A. Puliafito, and J. G. Fujimoto, "Optical coherence tomography," Science, **254**, 1178–1181 (1991).
3. G. J. Tearney, M. E. Brezinski, J. F. Southern, B. E. Bouma, M. R. Hee, and J. G. Fujimoto, "Determination of the refractive index of highly scattering human tissue by optical coherence tomography," Opt. Lett. **20**(21), 2258–2260 (1995).
4. T. Fukano, and I. Yamaguchi, "Simultaneous measurement of thickness and refractive indices of multiple layers by a low-coherence confocal interference microscope," Opt. Lett. **21**(23), 1942–1944 (1996).
5. M. Haruna, M. Ohmi, T. Mitsuyama, H. Tajiri, H. Maruyama, and M. Hashimoto, "Simultaneous measurement of the phase and group indices and the thickness of transparent plates by low-coherence interferometry," Opt. Lett. **23**(12), 966–968 (1998).
6. H. Maruyama, T. Mitsuyama, M. Ohmi, and M. Haruna, "Simultaneous measurement of refractive index and thickness by low-coherence interferometry considering chromatic dispersion of index," Opt. Rev. **7**(5), 468–472 (2000).
7. M. Ohmi, H. Nishi, Y. Konishi, Y. Yamada, and M. Haruna, "High-speed simultaneous measurement of refractive index and thickness of transparent plates by low-coherence interferometry and confocal optics," Meas. Sci. Technol. **15**, 1531-1535 (2004).
8. S. Kim, J. Na, M. J. Kim, and B. H. Lee, "Simultaneous measurement of refractive index and thickness by combining low-coherence interferometry and confocal optics," Opt. Express **16**(8), 5516–5526 (2008).
9. J. Na, H. Y. Choi, E. S. Choi, C. S. Lee, and B. H. Lee, "Self-referenced spectral interferometry for simultaneous measurements of thickness and refractive index," Appl. Opt. **49**(13), 2461–2467 (2009).
10. S. J. Park, K. S. Park, Y. H. Kim, and B. H. Lee, "Simultaneous measurements of refractive index and thickness by spectral-domain low-coherence interferometry having dual sample probes," IEEE Photonic. Tech. L. **23**(15), 1076-1078 (2011).
11. B. Hussain, M. Ahmed, M. Nawaz, M. Saleem, M. Razzaq, M. Aslam Zia, and M. Iqbal, "Simultaneous measurement of thickness and refractive index based on time-of-flight measurements of terahertz pulse," Appl. Opt. **51**(21), 5326–5330 (2012).
12. J. Yao, J. Huang, P. Meemon, M. Ponting, and J. P. Rolland, "Simultaneous estimation of thickness and refractive index of layered gradient refractive index optics using a hybrid confocal-scan swept-source optical coherence tomography system," Opt. Express **23**(23), 30149–30164 (2014).

#309958 https://doi.org/10.1364/OE.26.003604
Journal © 2018 Received 25 Oct 2017; revised 1 Dec 2017; accepted 2 Dec 2017; published 2 Feb 2018

Optics EXPRESS

13. S. C. Zilio, "Simultaneous thickness and group index measurement with a single arm low-coherence interferometer," Opt. Express Opt. Express **22**(22), 27392–27397 (2014).
14. C. Moreno-Hernández, D. Monzón-Hernández, I. Hernández-Romano, and J. Villatoro, "Single tapered fiber tip for simultaneous measurements of thickness, refractive index and distance to a sample," Opt. Express **23**(17), 22141-22148 (2015).
15. S-W. Cho, G. H. Kim, M. Kim, B. S. Shin, and C-S. Kim, "Line-field swept-source interferometer for simultaneous measurement of thickness and refractive index distribution," J. Lightwave Technol. **35**(16), 3584-3590 (2017).
16. T. Boettcher, M. Gronle, and W. Osten, "Multi-layer topography measurement using a new hybrid single-shot technique: Chromatic Confocal Coherence Tomography (CCCT)," Opt. Express **25**(9), 10204–10213 (2017).
17. K. J. Larkin, "Efficient nonlinear algorithm for envelope detection in white light interferometry," J. Opt. Soc. Am. A **13**(4), 832–843 (1996).
18. P. Liu, R. M. Groves, and R. Benedictus, "Signal processing in optical coherence tomography for aerospace material characterization," Opt. Eng. **52**(3), 033201 (2013).
19. D. C. Adler, *Digital signal processing techniques for optical coherence tomography: spectroscopic OCT and OCT image enhancement*, MSc. Thesis, Massachusetts Institute of Technology (Cambridge, MA. 2014).
20. P Pavliček and S Svak, "Noise properties of Hilbert transform evaluation," Meas. Sci. Technol. **26**, 085207 (2015).
21. M. N. Polyanskiy, "Refractive index database," `https://refractiveindex.info`
22. M. Daimon and A. Masumura, "High-accuracy measurements of the refractive index and its temperature coefficient of calcium fluoride in a wide wavelength range from 138 to 2326 nm," Appl. Opt. **41**(25), 5275–5281 (2002).
23. I. H. Malitson, "Interspecimen comparison of the refractive index of fused silica," J. Opt. Soc. Am. **55**(10), 1205–1209 (1965).
24. Schott, Optical glass datasheets, (July 2015).
25. Schott UK, Skan House, Stratford Road, Shirley, Solihull, West Midlands. B90 4AE, UK (personal communication, December 2016).

1. Introduction

It has long been known that low-coherence interferometry can be used to measure the thickness of transparent media [1]. In fact, the extension of low-coherence interferometry for micrometre scale ranging from a point measurement to a planar measurement led to the development of optical coherence tomography (OCT), which has become widely used for subsurface imaging of semi-transparent biological structures [2]. The thickness values obtained by low-coherence techniques are optical thicknesses, therefore a measure of the refractive index n is required to obtain the geometrical thickness t. Refractive index measurement using OCT has been demonstrated in-vitro on human tissue by scanning the sample through the focus of a lens in the sample arm of the interferometer [3], however to independently measure both the phase and group refractive indices n_p and n_g, together with t, additional measurements are required. One way of achieving this is to combine low-coherence interferometry with confocal scanning microscopy, which is a technique that was developed in Japan from the late 1990s.

The first demonstration of this combination of techniques used a multi-layered test object consisting of a series of glass cover slips with an air gap between them [4]. These were used to measure the phase refractive index n_p and the geometrical thickness but not the dispersion dependent group refractive index n_g, which was previously assumed to be equivalent to n_p for cases where the chromatic dispersion $dn/d\lambda$ is small. Where this assumption does not hold, significant error will be introduced into the measurement. To obtain n_g in addition to n_p and t, Haruna *et al*. [5] modified the technique to use a special holder consisting of pair of glass plates with a known separation between them to hold the sample. The sample holder was complex to set up and requires measurements of the glass plate interfaces as well as those of the sample. However, they were able to measure the three quantities n_p, n_g, and t to accuracies of ~0.3%. They were later able to simplify the measurement by using an approximated dispersion term with the sample holder used only for calibration [6]. A later publication demonstrated reduction of the measurement time by using a dual-channel interferometer to simultaneously measure both the low-coherence signals and the confocal scanning signals [7].

In 2008, Kim *et al*. [8] demonstrated two alternative methods to measure n_p, n_g, and t which improved on the accuracy of those presented previously. The more successful of the two techniques

Optics EXPRESS

involved measuring the chromatic dispersion directly by making the measurements at multiple wavelengths. This was achieved by using broadband SLDs with different centre wavelengths. A later publication from the same group demonstrated improved accuracy and repeatability of measurements of n_g and t using a self-referenced spectral domain interferometer [9]. This improvement was largely due to the required data being acquired in a single spectrum eliminating drift in the system. They later adapted this spectral domain system to use dual-probe beams illuminating the object from either side [10]. This adaptation had the additional benefits of requiring no moving parts and the ability to measure very highly absorbing materials.

Other alternative but related techniques described more recently to measure thickness and refractive index include; time-of-flight measurement of terahertz pulses [11], combined confocal scanning with swept-source OCT [12], single-channel low-coherence interferometry for measurement of t and n_g which requires no moving parts [13], and tapered-fibre Fabry-Perot interferometry [14]. The accuracy of these different techniques varies, however they do have other particular advantages such as the ability to measure semi-opaque or opaque materials [10, 11], improved immunity to mechanical vibration and drift [13], or improved accuracy for thin samples [14]. Further recent advances include two-dimensional measurement of group refractive index and thickness distribution using line-field swept-source interferometry [15] and the combination of chromatic confocal and interferometric techniques for single-shot refractive index and thickness measurement [16].

In this paper, the measurement of thickness and refractive index using a low-coherence interferometer with a high-speed CMOS line-scan spectrometer is described. The measurement principle is similar to that of Kim *et al*. [8] in that we measure the chromatic dispersion directly to obtain n_p, n_g, and t. The novelty of the technique presented here lies in the use of the spectrometer which allows measurement of the n_p dependent quantity at different wavelengths. This enables the measurement of the required dispersion term using a single source that is centred on the wavelength at which the confocal and low-coherence measurements are made. This development significantly simplifies the measurement procedure and provides a much higher resolution measurement of the dispersion curve at the wavelength of interest. This is of particular importance in cases where the material dispersion is not necessarily known, such as in the measurement of biological samples.

2. Interferometer configuration and spectrometer calibration

The optical system consists of a broadband light source, a fibre-optic coupler and a pair of translation stages. The test object is mounted on one translation stage which is scanned to make the confocal measurement and a mirror is mounted on the other stage which is scanned to make the low-coherence measurement. The optical configuration is shown in Fig. 1. The light source is a Superlum M-T-850-HP-I Broadlighter system which incorporates three super-luminescent diodes (SLDs) centred at approximately 780 nm, 840 nm, and 900 nm. Only the SLD centred at 840 nm was used here due to the limited bandwidth of the spectrometer as discussed below. Each SLD has a bandwidth of approximately 50 nm providing a total wavelength coverage of almost 150 nm. The maximum combined power of the source is 30 mW. The individual spectra for each SLD measured on a Yokogawa AQ6370C optical spectrum analyser are shown in Fig. 2(a). A Thorlabs TW850R2A2 broadband fibre-optic coupler is used to divide the light into sample and reference channels, with 90% of the light directed towards the sample and 10% towards the reference mirror. The ends of the fibre arms are terminated with 8° angled physical contact (APC) connectors. The fibre core in this system acts as the confocal aperture (diameter 4.4 μm) providing a system input numerical aperture (NA) of 0.13. Light exiting the fibre arms is collimated using Thorlabs AC080-020-B-ML achromatic doublets with 8 mm aperture diameter and 20 mm focal length. The lenses used to focus light onto the sample and the reference mirror are Thorlabs AC080-016-B-ML achromatic doublets with 8 mm aperture diameter and 16 mm

Optics EXPRESS

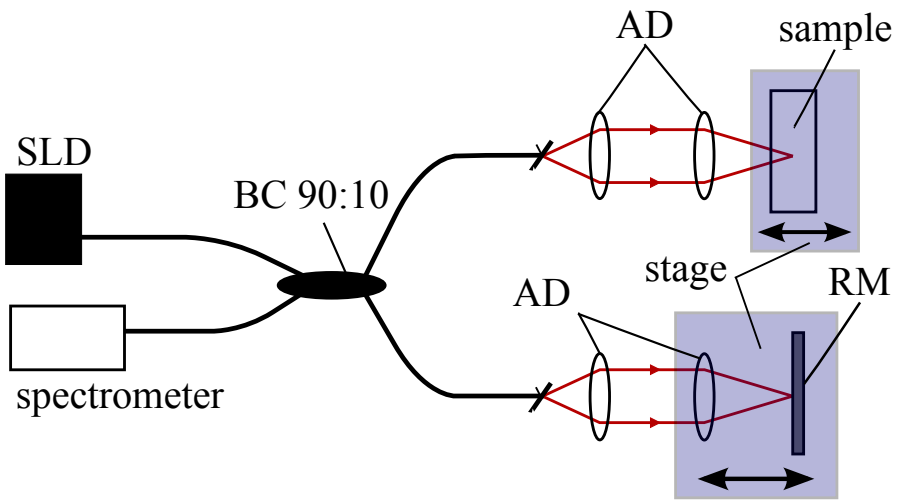

Fig. 1. Schematic showing the optical arrangement of the interferometer. SLD is the 840 nm centre wavelength super-luminescent diode, BC is the broadband coupler, RM is the reference mirror, and AD are 8 mm aperture achromatic doublets (20 mm focal length to collimate, 15 mm focal length to focus). The blue shading indicates which components are mounted on the translation stages in each arm.

focal length. The sample is mounted on a kinematic mirror mount with tip and tilt adjustment which is held on a Physik Instrumente M-110.1DG linear translation stage using a 3D printed adaptor plate. A similar translation stage and adaptor plate is used to hold the focusing lens and mirror in the reference arm of the interferometer. The translation stages have a maximum travel of 5 mm, a maximum velocity of 0.5 mm·s^{-1}, and a minimum incremental motion of 50 nm. The spectrometer is a BaySpec OCT Spectrograph @850nm system which incorporates a Basler spL4096-140km line-scan CMOS camera with an array size of 4,096 pixels and 12-bit digital resolution. A PC running LabVIEW software is used for control and data acquisition. The camera is interfaced to the PC using a National Instruments PCIe-1433 full Camera-Link frame grabber and the translation stages are controlled using a C-843 DC-servo-motor controller.

The effective bandwidth of the spectrometer is approximately 50 nm and therefore insufficient to capture information across the full spectral range of all three of the SLDs within the Superlum system, as shown in Fig. 2(b), therefore only SLD 2 was used in this work. The wavelength values of the spectrometer pixels were calibrated using an Ando AQ-4304 programmable light source. This device consists of a tungsten halogen lamp with a grating and slit monochromator and emits light at wavelengths from 600 - 1,600 nm at 1 nm intervals with bandwidths up to 15 nm. Light from the source was coupled directly to the spectrometer via a fibre-optic patch cable (single-mode, 720 nm cut-off wavelength) and incremented in 5 nm steps over the detectable range from 805 - 855 nm. The spectrometer signal was integrated for 2 minutes to maximise the response, shown in Fig. 3(a). A polynomial fit was applied to the recorded data for each wavelength in order to determine the pixel location of the peak of the curve. An eighth order polynomial was used which had a mean absolute residual of 1.70 across each of the datasets. This was the closest fit that could achieved before it starts to become visibly affected by the noise in the signal. The centre values of each of the wavelengths used were verified using an Ocean Optics HR4000 spectrometer and found to be underestimated by 0.4 nm which is well within the light source's quoted uncertainty of ±5 nm. The spectrometer wavelength variation was found to be linear over this range which corresponds to approximately pixel 900 to pixel 2,100 out

Optics EXPRESS

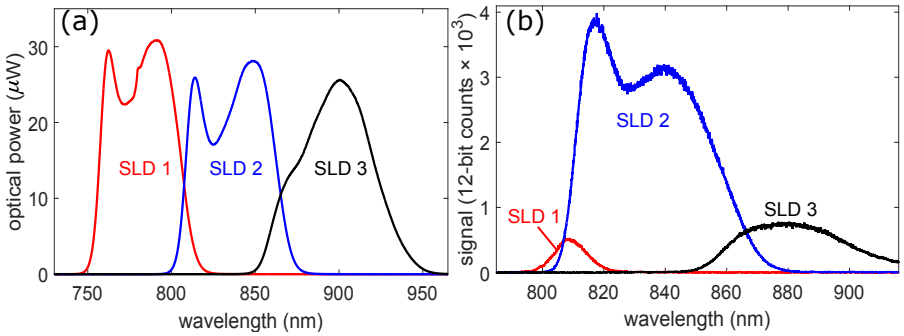

Fig. 2. Plots showing the spectra of the three SLDs present in the Superlum M-T-850-HP-I SLD system measured on (a) a Yokogawa AQ6370C optical spectrum analyser (0.2 nm resolution bandwidth) and (b) the BaySpec CMOS spectrometer (0.1 nm resolution bandwidth) used in the present work.

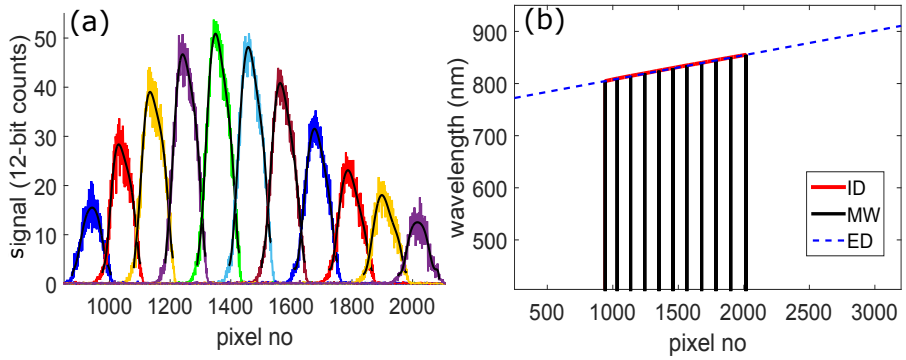

Fig. 3. Calibration procedure for the spectrometer: (a) Signals obtained after a two minute integration time for a range of wavelengths from 805 nm - 855 nm plotted against pixel number. Peaks were obtained sequentially but are shown here plotted on the same graph. The black curves are polynomial fits to the signal data. (b) Interpolation and extrapolation of the measured data to cover the entire 4,096 pixel array of the line-scan camera (only a section shown in the plot for illustration). ID = interpolated data, MW = measured wavelengths, ED = extrapolated data.

of the 4,096 pixel array. This linearity was used to interpolate the wavelength values between those measured and to extrapolate to cover the full range of the spectrometer array, as shown in Fig. 3(b).

3. Measurement principles

The measurement procedure is formed of two distinct parts; the confocal measurement and the low-coherence measurement. The non-interferometric confocal measurement is made by scanning the sample through the focus of the lens. A pair of reflection peaks, observed in the integrated signal, are associated with the front and rear surfaces of the object. Ignoring spherical aberration caused by the front sample surface, the separation of these peaks Δz is related to the

Optics EXPRESS

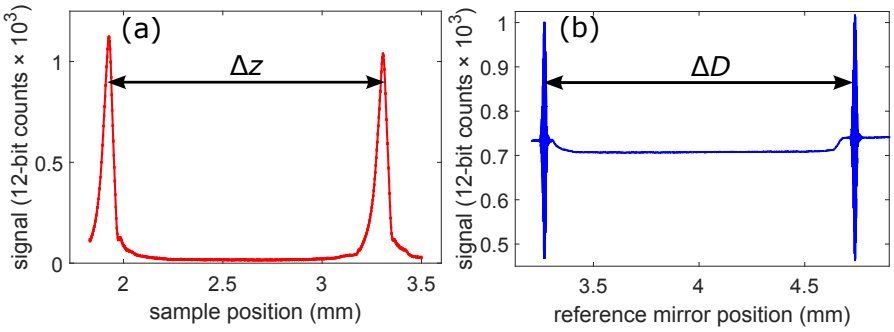

Fig. 4. Plots showing the measured quantities (a) Δz, the separation between the reflection peaks in the confocal arrangement, and (b) ΔD, the separation between the low-coherence fringe envelopes. These measurements were obtained using a CaF_2 window with a thickness of approximately 2 mm.

thickness t and the phase index n_p by [8]

$$\Delta z = t \times \frac{\sqrt{n_{air}^2 - NA^2}}{\sqrt{n_p^2 - NA^2}} \approx \frac{t}{n_p} \tag{1}$$

where NA is the numerical aperture of the focusing lens in the sample arm and n_{air} is the refractive index of air and is taken to be 1.0003 in this work. Figure 4(a) shows an example of the confocal refection peaks obtained when an approximately 2 mm thick CaF_2 window is scanned in the sample arm. The low-coherence measurement is made by focusing close to the rear surface of the sample and scanning the reference mirror through the point of zero optical path difference between the interferometer arms so that a burst of fringes is seen in the integrated signal. The sample is then translated so that the focus is now on the front surface and the reference mirror is again scanned through the point of path matching. The desired quantity Δl is the sum of the separation of the fringe envelopes ΔD, shown in Fig. 4(b), and the magnitude of the translation of the sample Δz. Δl is the optical thickness of the sample and relates n_g and t by

$$\Delta l = \Delta D + \Delta z = t \times n_g \tag{2}$$

If the sample is thin enough that light from both surfaces can be detected when the focus is placed between them then Δl can be obtained directly without the need to translate the sample. However, the fringe contrast is maximized by translating the sample to focus on each surface in turn, which is very important when making high accuracy measurements. The reduction in the mean signal seen between the two fringe envelopes in Fig. 4(b) is due to the sample translation since, while the majority of the received intensity comes from the reference mirror, there is still a noticeable contribution from the sample surface reflection which is lost during this translation between surfaces.

The group index depends on the chromatic dispersion, given by

$$n_g(\nu) = n_p(\nu) + \nu \frac{dn_p(\nu)}{d\nu} \tag{3}$$

where ν is the optical frequency. In the case that $NA^2 << 1$, the approximation given in Eq. (1) can be used. Substituting this and Eq. (2) into Eq. (3) yields

$$t^2 = \frac{\Delta l \Delta z}{1 - \frac{\nu}{\Delta z}\frac{d\Delta z}{d\nu}} \tag{4}$$

Optics EXPRESS

The thickness therefore depends on a dispersion term $\mathrm{d}\Delta z/\mathrm{d}z$ which can be acquired by making the confocal measurement at multiple wavelengths. This can be done by interrogating different regions of the spectrometer array separately, as will be discussed in section 4.2. The width of the reflection peaks in the confocal signal is approximately inversely proportional to the square of the numerical aperture of the focusing lens and to make accurate measurements of Δz, narrow peaks are generally desirable. Beams with a relatively high numerical aperture therefore need to be used. This is especially true when measuring thin objects where the peaks associated with the two surfaces need to be adequately resolved. Unfortunately, this means that the NA-independent assumption used to derive Eq. (4) cannot be used without introducing appreciable error. The full solution using Eq. (1) results in a more complex polynomial expression [8]

$$At^2 + Bt^4 + Ct^6 = 0$$

where

$$\begin{aligned} A &= \frac{\left(n_{\mathrm{air}}^2 - NA^2\right)^2}{\Delta z^4} + \nu^2 \frac{\left(n_{\mathrm{air}}^2 - NA^2\right)^2}{\Delta z^6}\left(\frac{\mathrm{d}\Delta z}{\mathrm{d}\nu}\right)^2 - 2\nu\frac{\left(n_{\mathrm{air}}^2 - NA^2\right)^2}{\Delta z^5}\frac{\mathrm{d}\Delta z}{\mathrm{d}\nu} \\ B &= 2\frac{\left(n_{\mathrm{air}}^2 - NA^2\right)}{\Delta z^2}NA^2 - 2NA^2\nu\frac{\left(n_{\mathrm{air}}^2 - NA^2\right)}{\Delta z^3}\frac{\mathrm{d}\Delta z}{\mathrm{d}\nu} \\ C &= NA^4 - \frac{\Delta l^2}{\Delta z^2} - \left(n_{\mathrm{air}}^2 - NA^2\right) \\ D &= -\Delta l^2 NA^2 \end{aligned} \tag{5}$$

Once t has been obtained using equation (5), n_{p} and n_{g} can be calculated using equations (1) and (2).

4. Confocal and low-coherence measurements

This section describes the data acquisition procedure in more detail and the processing steps taken to determine the three desired quantities Δl, Δz, and $\mathrm{d}\Delta z/\mathrm{d}\nu$. The computer program used to control the spectrometer's line-scan camera and the translation stages was also used to record averaged spectrometer data and stage positions as the measurements were being made. The location of the sample for each spectrometer acquisition was made by comparing the timestamp of each acquisition with that of each of the stage position measurements. There is a certain delay associated with the call to the stage position feedback function that limits the data rate to approximately 10 Hz. The spectrometer is capable of significantly higher acquisition rates than this, therefore linear interpolation assuming a constant stage velocity was applied to determine the locations for spectrometer acquisitions made between consecutive position readings. The spectrometer acquisition rate was set to 500 Hz and the stage position feedback rate was set to 10 Hz for both low-coherence and confocal measurements.

4.1. Measurement of Δl

The measurement of Δl requires the determination of the locations of the peaks of the low-coherence fringe envelopes associated with each surface of the sample. The received light from the reference mirror was significant, therefore the spectrometer acquisitions were made with the shortest possible exposure time of 15 µs to ensure that the brightest parts of the spectrum were not overexposed. Additionally, an aperture was used in the reference arm to sufficiently attenuate the light. The approximate reference mirror locations corresponding to interferometric path matching for both surfaces were determined prior to making a measurement. The reference mirror was then placed 35 µm before the point of path matching and scanned at a velocity of 2 µm·s^{-1} for 70 µm, which is sufficient distance to cover the entire peak envelope. The object

Optics EXPRESS

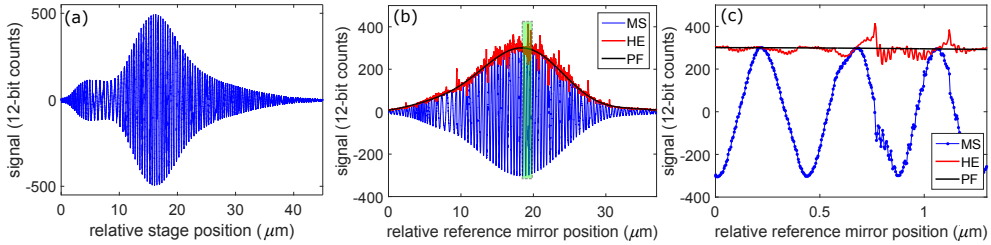

Fig. 5. Plots showing low-coherence fringe envelopes obtained with the system: (a) shows the influence of the spectral intensity distribution (shown in Fig. 2(b)) on the fringe pattern obtained using the SLD, (b) shows a fringe pattern obtained with each individual spectrometer acquisition multiplied by a Gaussian function and the demodulated fringe envelope (MS = mean integrated signal, HE = Hilbert envelope, PF = polynomial fit). The highlighted region near the centre shows the section of the fringe pattern used to plot (c), which shows that the noise in the Hilbert envelope corresponds with noise in the integrated signal.

was then translated at the full stage velocity until the opposite surface was in the focal plane of the lens and the process was repeated.

The shape of the fringe envelope is dependent on the spectral distribution of intensity recorded by the camera and it is desirable for this to be symmetric to accurately determine the peak location. The fringe pattern obtained using the system is shown in Fig. 5(a) and is non-symmetric due to the spectral intensity distribution as seen in Fig. 2(b). Therefore, to force fringe pattern symmetry the individual spectrometer acquisitions are multiplied by a Gaussian function which results in fringe patterns with a form like that shown in Fig. 5(b). To find the centre of the fringe burst, it is necessary to demodulate the fringe envelope and a well-established method of achieving this is to use the Hilbert transform [17, 18]. This technique is advantageous because it does not require the phase and frequency of the fringe pattern to be constant over time [19]. After subtracting the mean value from a signal, the envelope can be acquired from the magnitude of the analytic signal $\left(\sqrt{\mathrm{Re}^2 + \mathrm{Im}^2}\right)$, where the real part contains the original signal and the imaginary part contains the Hilbert transform. The demodulated Hilbert envelope of the fringe pattern, is shown as the red trace in Fig. 5(b). The Hilbert envelope is affected by noise that is present in the interferogram data [20] and this can be seen more clearly by looking at the fringe data on a much shorter time-scale, as shown in Fig. 5(c) where the largest noise spikes in the envelope correspond with the parts of the interferogram signal that are most corrupted by noise. The value that is required for Δl is the stage position at which the envelope signal is a maximum, which is determined from a polynomial fit to the envelope data.

4.2. *Measurement of* Δz *and* $\mathrm{d}\Delta z/\mathrm{d}\nu$

The non-interferometric confocal measurements are made to find Δz, the separation between the reflected peaks, as the sample is scanned through the focus of the lens in the sample arm of the interferometer. To determine t using equation (5) the dispersion term $\mathrm{d}\Delta z/\mathrm{d}\nu$ is also required, therefore the measurements were made at multiple wavelengths simultaneously. The reference mirror was blocked with a black card so that only light reflecting from the sample was detected. The received light from the sample surfaces is dependent on the material, therefore the spectrometer exposure time was set at different durations ranging from approximately 100 μs to 300 μs for each sample type, to maximise the signal recorded by the camera without overexposing. Figure 6(a) shows an example of a confocal measurement on a BK7 window. As the object was scanned, each spectrometer acquisition was divided into sub-regions with a width of 65 pixels and a centre separation of 16 pixels, and the Gaussian weighted mean was calculated for each.

Optics EXPRESS

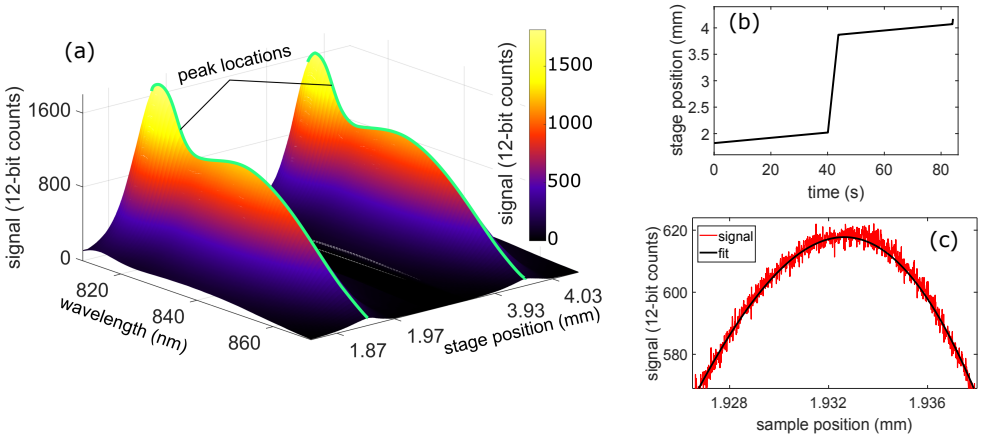

Fig. 6. Multi-wavelength confocal measurement of a BK7 window: (a) plot showing the reflected signal from both surfaces of the BK7 window as the object is scanned through the focus of the sample arm lens. (b) The path traversed by the stage. (c) The top of the reflected peak associated with the front surface at 850 nm and the polynomial fit to the data.

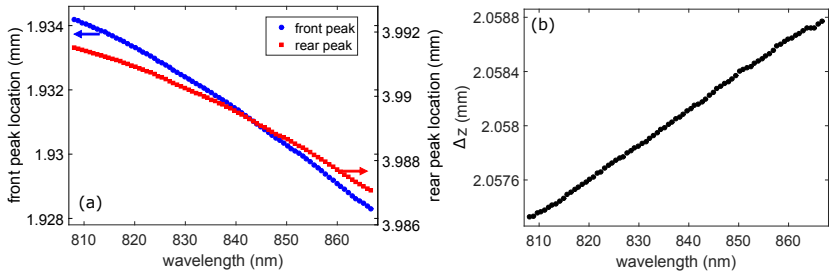

Fig. 7. (a) Plots showing the variation in peak position with wavelength for the front and rear surfaces. (b) The difference between peak locations at each wavelength, the gradient of which provides the dispersion term $\mathrm{d}\Delta z/\mathrm{d}\nu$.

This reduces noise and the overall data load and results in 89 individual measurements of Δz at different wavelengths. The plot shows the integrated signal for each of the wavelength sub-regions plotted against stage position as it traverses the path. The separation between the front and rear peaks is much larger (~3 mm) than the peak widths (~10 μm) so has been reduced in the plot for clarity. Both surfaces of the object were scanned through focus using a pre-programmed path with a velocity of 5 μm·s^{-1} in the vicinity (±100 μm) of the peaks and at the maximum velocity (5 mm·s^{-1}) between the surfaces. The path traversed by the stage is shown in Fig. 6(b).

To determine Δz, the peak locations at each wavelength need to be found to a high accuracy. There is some random noise associated with the reflected peak data as can be seen in Fig. 6(c), which shows the top of the front peak at a wavelength of 850 nm, therefore a polynomial fit was used to obtain the peak position. The peak locations for both front and rear surfaces at each wavelength measured are shown in Fig. 7(a). The difference between them provides Δz at each wavelength, as shown in Fig. 7(b), and the gradient of this line yields the dispersion term $\mathrm{d}\Delta z/\mathrm{d}\nu$.

5. Refractive index and thickness measurements

The quantities obtained from the confocal measurement, Δz and $\mathrm{d}\Delta z/\mathrm{d}\nu$ are required to calculate the thickness t using equation (5). Additionally, the NA of the focusing lens needs to be known.

Optics EXPRESS

Since the diameter of the collimated beam is smaller than the aperture of the focusing lens and measuring it directly is difficult, the NA was calibrated using an object of known refractive index, in this case a BK7 window. This was done using equation (1) rearranged for NA

$$NA = \sqrt{\frac{n_{\text{air}}^2 t^2 - n_{\text{p}}^2 \Delta z^2}{t^2 - \Delta z^2}} \tag{6}$$

where n_{p} and t are the reference phase index and thickness values described below and Δz is measured experimentally using the method described in section 4.2. The NA was found to be 0.133 ± 0.001. The phase index is then calculated using equation (1) and the group index is obtained from the Δl measurement using equation (2).

To test the measurement technique, a set of five circular windows was acquired (Edmund Optics) each with a diameter of 20 mm. The windows were constructed from CaF_2, BK7, B270 (superwite), fused silica, and sapphire. They were all nominally 2 mm thick except for the BK7 window which was ~3 mm thick. In addition, a BK7 window with a nominal thickness of 200 μm was investigated to test the suitability of the technique for measuring thin samples. Measurement of thin samples requires the use of a relatively high NA lens in the confocal arm to provide sufficiently narrow depth of focus to adequately resolve the peaks. Additionally, good alignment is critical because any tilt of the object relative to the optical axis will introduce much larger percentage errors in the Δz and $\mathrm{d}\Delta z/\mathrm{d}\nu$ measurements than for thicker objects. Another issue is the interference present in the detected signal arising due to the etalon formed between the front and rear surfaces, which is not observable with the thicker objects but is significant with the thin sample. The interference introduces noise in the $\mathrm{d}\Delta z/\mathrm{d}\nu$ measurements but can be significantly reduced by removing the appropriate Fourier frequencies. Figure 8 shows the difference in the spectrometer acquisitions and the associated $\mathrm{d}\Delta z/\mathrm{d}\nu$ measurement with and without Fourier filtering.

Ten independent measurements of Δl, Δz and $\mathrm{d}\Delta z/\mathrm{d}\nu$ were made for each sample whereby the sample was removed and replaced between each successive measurement. Doing this helps to provide a better understanding of the repeatability of the technique. The mean refractive index measurements for the four non-birefringent materials are summarized in Table 1 along with the standard deviation of the ten measurements and the percentage error based on the difference of the mean measured value from the reference value. In most cases the percentage errors lie within the standard deviation of measurements.

Table 1. Summary of phase and group refractive index measurements for four different optical materials.

	Phase index (n_{p})				**Group index (n_{g})**			
Sample	**Ref**	**Meas**	**St Dev**	**Err(%)**	**Ref**	**Meas**	**St Dev**	**Err(%)**
CaF_2	1.4302	1.4286	0.0008	0.11	1.4380	1.4383	0.0016	0.02
B270	1.5161	1.5157	0.0011	0.02	1.5320	1.5288	0.0014	0.21
Fus Si	1.4527	1.4521	0.0007	0.05	1.4660	1.4666	0.0005	0.04
BK7	1.5100	1.5096	0.0003	0.03	1.5252	1.5250	0.0004	0.01
BK7 thin	1.5100	1.5126	0.0028	0.17	1.5252	1.5247	0.0028	0.03

The reference refractive index values were taken from the online database *refractiveindex.info* [21], which were obtained from a range of sources. Reference values were available for CaF_2 [22], fused silica [23], and BK7 [24] for particular wavelengths and determined for 840 nm using the Sellmeier equation. The reference values for B270 were obtained using Sellmeier coefficients provided in a private communication from Schott. Since B270 is not considered a high-spec optical glass, refractive index and dispersion measurements are not routinely made

Optics EXPRESS

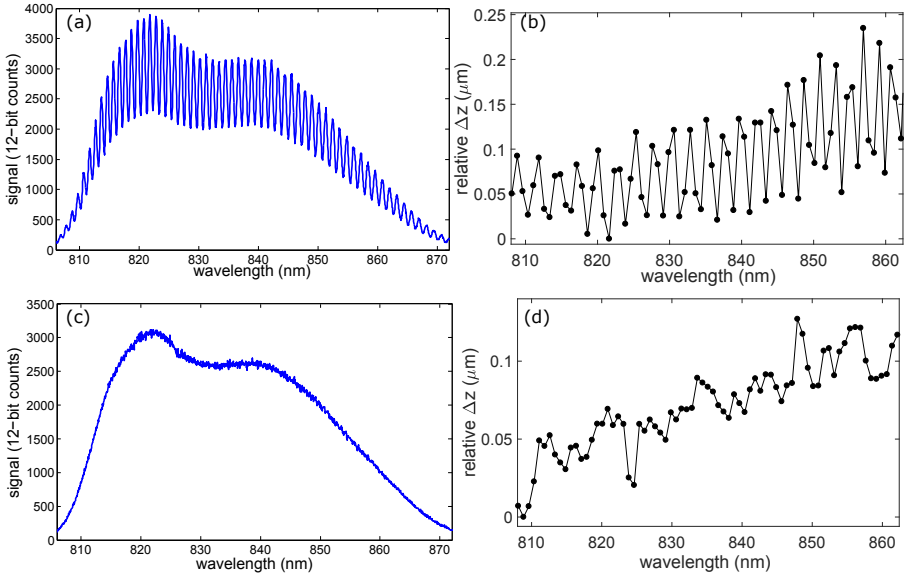

Fig. 8. The impact of etalon fringes present when measuring a thin BK7 window on the dispersion measurement and improvement through Fourier filtering: (a) a typical spectrometer acquisition at a confocal peak and (b) the associated dispersion measurement, (c) and (d) are similar plots obtained after using Fourier filtering to reduce the etalon fringes. Note the more readily discernible gradient of (d) relative to (b).

for each sample, these values are only indicative [25]. This may explain the somewhat larger error in the group index measurement relative to the other samples. The experimental difficulty in measuring the thin sample is reflected in the higher standard deviation and higher percentage error in the phase index relative to the other samples.

The measured thicknesses of the samples are summarized in Table 2. The reference thickness values were obtained using a Mitutoyo MDH digital micrometer gauge, which has a resolution of 0.1 μm. For each sample, ten independent measurements were made whereby the gauge was removed and re-zeroed between each successive measurement. The standard deviation associated with the micrometer gauge measurements is shown in the adjacent column in Table 2. The best accuracy and repeatability was generally obtained when using the BK7 window. The improved accuracy was likely due to the window being somewhat thicker than the others (~3 mm compared to ~2 mm) and the better repeatability because it is specified to a tighter flatness tolerance than the others ($\lambda/4$ compared to λ).

Table 2. Summary of thickness measurements for four different materials given in millimetres. The reference values were obtained using a micrometer gauge and were measured ten times, hence they have an associated standard deviation.

Sample	Ref	St Dev	Meas	St Dev	Err(%)
CaF_2	1.9818	0.0003	1.9818	0.0024	0.00
B270	2.0583	0.0008	2.0607	0.0021	0.11
Fus Si	2.3443	0.0016	2.3407	0.0008	0.15
BK7	3.1230	0.0002	3.1219	0.0006	0.03
BK7 thin	0.2162	0.0003	0.2155	0.0017	0.31

Sapphire is birefringent and therefore has two refractive indices associated with the ordinary

Optics EXPRESS

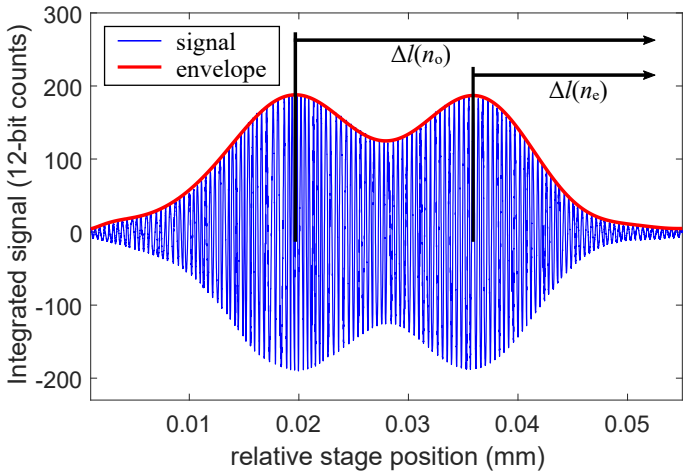

Fig. 9. Plot showing the fringe burst associated with the rear surface of a sapphire window. The integrated spectrometer data is plotted along with the polynomial fit to the demodulated Hilbert envelope. The arrows indicate the peak separations (from the fringe burst associated with the front surface) used to determine Δl for the ordinary and extraordinary refractive indices.

and extraordinary optical paths through the material. This results in a double peak in the fringe envelope associated with the low-coherence measurement of the rear surface. The presence of a double peak within the low-coherence envelope may indicate that the material under investigation is birefringent. The orientation of the window about the optical axis determines the relative magnitude of the two peaks, and can be rotated so that they are approximately equal, as shown in figure 9. The peak locations can be used to determine Δl for the ordinary and extraordinary refractive indices which, combined with the measurement of Δz, can be used to calculate the phase and group indices for both. The refractive index and thickness measurements are summarized in Table 3 and Table 4, respectively. Although the two peaks in the envelope are clearly distinguishable, there is significant overlap. This overlap may cause one peak to influence the other, displacing the peak position slightly. This may be affected by the relative magnitude of the peaks - which can be varied by rotating the sapphire plate about the optical axis - or by the envelope demodulation algorithm. This may explain the slightly larger error in the n_e measurements. This could be improved by using a wider source bandwidth to narrow the fringe envelopes.

Table 3. Measurements of the phase and group refractive indices for the ordinary and extraordinary optical paths of a birefringent sapphire window.

	Phase index (n_p)				**Group index(n_g)**			
Sample	**Ref**	**Meas**	**St Dev**	**Err(%)**	**Ref**	**Meas**	**St Dev**	**Err(%)**
Al_2O_3 (n_o)	1.7591	1.7583	0.0022	0.04	1.7797	1.7788	0.0015	0.05
Al_2O_3 (n_e)	1.7512	1.7544	0.0022	0.18	1.7715	1.7748	0.0015	0.19

Table 4. Measurements of the thickness of a sapphire window given in millimetres.

Sample	**Ref**	**St Dev**	**Meas**	**St Dev**	**Err(%)**
Al_2O_3	2.0208	0.0015	2.0192	0.0018	0.08

Optics EXPRESS

The mean percentage errors over all of the samples tested for the three measured components were 0.09% for n_p, 0.08% for n_g, and 0.11% for t. To put the performance of our technique into context with other published work, a summary of the mean percentage errors obtained for these components by other authors is shown in Table 5. These are the mean errors calculated for all the samples that were tested. These are provided for context only and it should be noted that improved accuracy is not necessarily the primary motivation for those publications referred to in the table.

Table 5. Summary of mean percentage errors in n_p, n_g, and t from various publications based on quoted data. '**S**' represents the number of samples tested.

Contribution	**Year**	**S**	n_p**(%)**	n_g**(%)**	t**(%)**	**Ref**
OCT for RI measurement[a]	1995	2	-	0.20	0.00	[3]
Low-coherence confocal microscopy	1996	2	0.10	-	0.80	[4]
Special sample holder[b]	1998	7	0.08	0.14	0.15	[5]
Approximated dispersion term[c]	2000	6	0.06	0.23	0.16	[6]
Multiple wavelengths to determine dispersion[d]	2008	8	0.07	0.06	0.06	[8]
Self-referenced spectral-domain interferometer[e]	2009	3	-	0.02	0.03	[9]
Dual-probe spectral-domain interferometry	2011	7	-	0.06	0.06	[10]
Time-of-flight measurement of terahertz pulses	2012	9	1.39	-	0.77	[11]
Single channel low-coherence interferometer	2014	3	-	0.22	0.35	[13]
Tapered fibre Fabry-Perot interferometer	2015	8	-	0.09	0.03	[14]
Spectrometer dispersion measurement (this work)[b]	2017	6	0.09	0.08	0.11	-

[a] Only non-biological samples taken into consideration.
[b] Ordinary and extraordinary refractive indices of birefringent material treated as two separate samples.
[c] Only measurements made with the approximated dispersion term taken into consideration.
[d] Only errors associated with the multi-wavelength approach quoted here. Does not include the errors for thinner samples.
[e] One sample measured at three different wavelengths. Only self-referenced measurements considered here.

6. Discussion and conclusions

A method of measuring the two refractive index components n_p and n_g, and the geometrical thickness t using combined low-coherence interferometry and confocal scanning has been presented. The technique relies on the measurement of dispersion which is achieved by measuring the confocal peak separation at different wavelengths across the bandwidth of a CMOS spectrometer. This represents an alternative to the previously demonstrated method of using multiple SLD sources [8], or values determined using known Sellmeier coefficients [6, 12]. The use of multiple sources requires repetition of the measurements for each of the sources used, and is therefore a more time-consuming and cumbersome approach. Also, with the spectrometer-based approach, the dispersion is measured over the range provided by the source bandwidth (i.e. ±25 nm) and is therefore much closer to the centre wavelength than it would be if a second source were used in a different wavelength region. This is beneficial because the magnitude of the chromatic dispersion itself varies with wavelength. In addition, the ability to measure chromatic dispersion directly, without relying on known constants, is particularly advantageous in instances where these values are not well-known, for example in the measurement of biomedical samples.

To measure the dispersion requires very accurate measurement of the confocal peak location at each of the different wavelengths measured across the spectrometer array. This requires very good alignment as well as good quality optics to minimise the impact of imaging aberrations. Additionally we have found that the choice of the numerical aperture of the focusing lens is also important. Too low an NA introduces too much broadening of the confocal peaks resulting in less accurate determination of the peak location. On the other hand, too high an NA can result in distortions of the peak introduced due to aberrations since the confocal peak is essentially a one-dimensional measure of the axial point-spread function of the focusing lens. The NAs that

Optics EXPRESS

were tried ranged from approximately 0.09 to 0.16 with the best performance obtained using an NA of 0.133.

The measurement time for either the confocal or low-coherence scan was of the order of a minute for each of the results presented here, however for this work the stages were run relatively slowly in order to maximise the number of data points for each scan. It is anticipated that this time can be reduced by an order of magnitude or more whilst still retaining good measurement accuracy by increasing the stage velocity in the vicinity of the interfaces.

Funding

Engineering and Physical Sciences Research Council (EPSRC grant EP/M010473/1).

Acknowledgment

The underlying data can be accessed through the Cranfield University data repository at 10.17862/cranfield.rd.5519725

Spectrometer-based refractive index and dispersion measurement using low-coherence interferometry with confocal scanning

Francis, Daniel

2018-02-02

Daniel Francis, Helen D. Ford and Ralph P. Tatam. Spectrometer-based refractive index and dispersion measurement using low-coherence interferometry with confocal scanning. Optics Express, 2018, Vol. 26, Issue 3, pp. 3604-3617

https://doi.org/10.1364/OE.26.003604